Int. J. Heat Mass Transfer. Vol. 23, pp. 805–811

0017 9310/80/0601 0805 $02.00/0

MASS TRANSFER TO ROTATING RODS AND PLATES

I. CORNET, R. GREIF, J. T. TENG* and F. ROEHLER†
Department of Mechanical Engineering, University of California, Berkeley, CA 94720, U.S.A.

(*Received* 31 *July* 1979 *and in revised form* 19 *November* 1979)

Abstract—Experimental results are presented for the mass transfer to rotating rods and plates. Flow regimes and their effect on the mass transport are noted. A calculation procedure based on a cross-flow stationary-cylinder analogy is presented and compared with the experimental data.

NOMENCLATURE

- B, width of rotating plate [m];
- D, rod diameter [m];
- $\mathscr{D}$, molecular diffusion coefficient [m^2/s];
- H, thickness of rotating plate [m];
- L, half length of rotating rod (or plate) [m];
- L_0, radius of supporting shaft [m];
- Re, Reynolds number, $(L+L_0)\omega D/2\nu$ or $(L+L_0)\omega B/2\nu$;
- Re_L, Reynolds number for rod based on L, $L\omega D/\nu$;
- Re_{L_0}, Reynolds number for rod based on L_0, $L_0\omega D/\nu$;
- Sc, Schmidt number, $\nu/\mathscr{D}$;
- Sh, overall or average Sherwood number;
- u, local rotational velocity [m/s];
- x, distance measured along the rod (or plate) away from the supporting shaft [m].

Greek symbols

- ν, kinematic viscosity [m^2/s];
- ω, angular velocity, rpm.

INTRODUCTION

A NUMBER of studies have been carried out to determine the heat and mass transfer in rotating flows. Because of the complex nature of rotating-flow fields, and the attendant difficulty in determining the heat and mass transport, there has been an emphasis on studies of comparatively simple configurations, viz. disks, cylinders, cones, etc. rotating about their axes of symmetry. The purpose of the present investigation was to provide results for the mass transfer for more complex systems.

EXPERIMENTAL SYSTEM

Measurements were made of the mass transfer to three vertically mounted brass shapes: a 3.81 cm diameter cylinder or rod 36.83 cm long, a flat plate or blade 0.635 cm by 5.08 cm by 36.83 cm, and a pitched plate with the same dimensions as the foregoing but with a 10° pitch. Each was mounted separately in a 6.35 cm diameter acrylic–plastic cylinder with a brass female mounting shaft which mated to the male main drive shaft (cf. Figs. 1 and 2). The test specimens, immersed in 113 l. of 3.5% NaCl aqueous solution with a 25.4 cm head, were made cathodic and rotated horizontally about the shaft perpendicular to its long axis. The anode of the system was a thin circular sheet of titanium located at the bottom of the 113 l. container and 50 cm from the propeller. A compressed Micarta material 1 cm thick was used to fabricate baffles to reduce the core velocity of the solution. The baffles were cut away to provide 5.1 cm tip clearance for all the rotating shapes. Vertical clearances, on the top and on the bottom, were 2.6 cm for the rod, 4.2 cm for the flat plate and 4.0 cm for the pitched plate.

The reference electrode for the system was a silver–silver chloride cell. The control potential and current source were provided by a Brinkmann Wenking potentiostat.

Drive for the specimens was a 1/2 horsepower AC motor. The speed of rotation of the specimen was measured from a 60-tooth gear on the main drive shaft by a magnetic pickup, an amplifier, and an electronic digital counter.

Details of the experimental system are shown in Fig. 3. Additional information on the electrochemical technique may be found in Levich [3], Tobias *et al.* [4], Delahay [5], Newman [6], and Teng *et al.* [7].

Procedure

The 3.5% NaCl solution was mixed before the experiment and stored overnight in a plastic-covered tank to allow the solution to reach a steady state with respect to the dissolved oxygen concentration. Fifty gallons of city tap water were mixed with 15.1 lb of reagent grade NaCl to give a 3.5% solution. The electronic counter and Wenking potentiostat were turned on and left in standby to warm up.

In order to maintain a reproducible surface, each day the surface of the propeller used was polished with a metal polish, washed with detergent and city tap water and rinsed in tap water. The propeller was then inserted through the center hole in the Plexiglas lid and

* General Electric Company, San Jose, CA, U.S.A.
† U.S. Naval Civil Engineering Laboratory, Port Hueneme, CA, U.S.A.

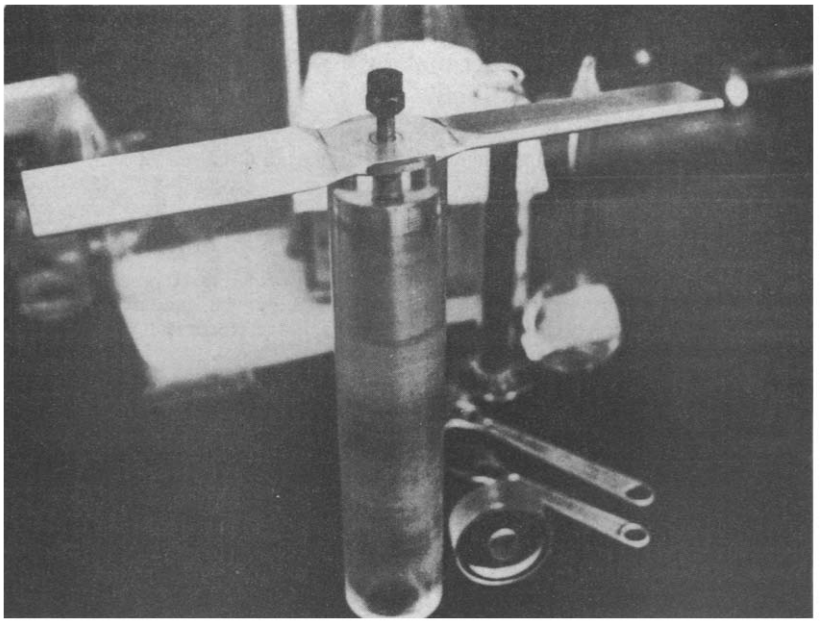

FIG. 1. Partial disassembly of pitched flat plate.

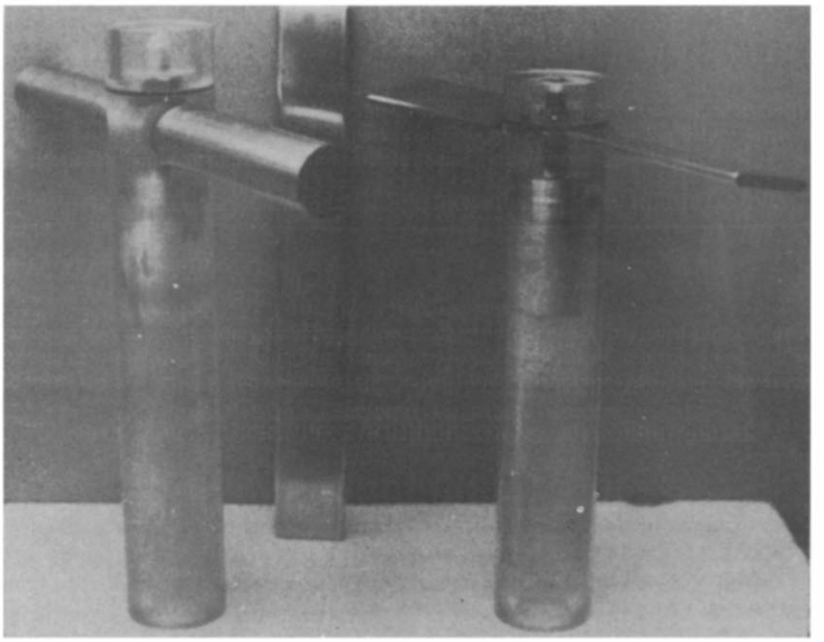

FIG. 2. Cylindrical rod, flat plate and pitched flat plate.

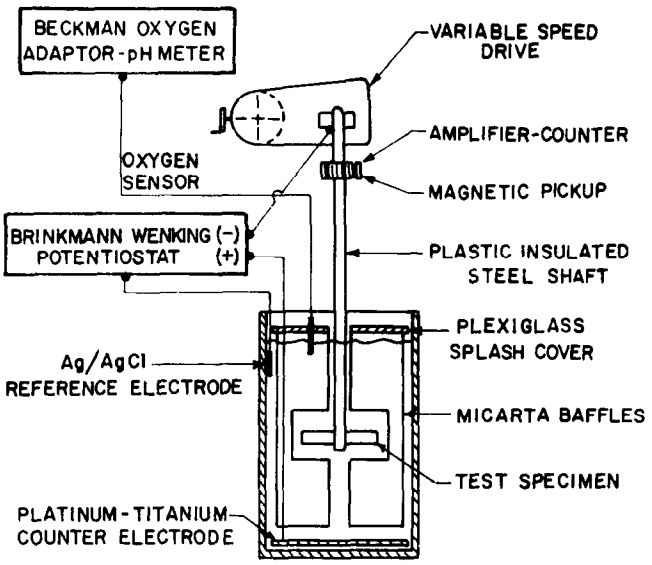

FIG. 3. Experimental system.

threaded hand-tight on the main-drive shaft. The entire drive apparatus was mounted on an elevated platform and the working tank/baffle/counter electrode assembly was positioned under the propeller. The tank assembly was then slowly raised by a lift stacker until the propeller was inside the tank. Oxygen was determined by use of a Beckman Oxygen Adapter and Expandomatic pH meter assembly.

The first part of the experimental work was to obtain a plot of the potential vs current curve so that the mass-transfer limiting current and its associated potential could be determined. This was accomplished by setting potentials of from 700 mV to 1400 mV on the vernier of the potentiostat and switching to I, the actual working position of the potentiostat, to record the current. The first run was made at a constant 43 rpm so that a uniform polarization would take place. The system was then stopped and a second run of from 500 mV to 1250 mV was recorded. The initial polarization of the propeller was then read as current vs time. The potentiostat was then set at 1000 mV.

After the current reached a slowly declining value of 0.2 mA per 30 s period, the apparatus was started at the lowest rpm and the current read. For small increments in rpm, there was no change in the value of the current vs time, so that the reading of current could be taken directly after the reading of rpm. The initial and final temperatures and specific gravity were recorded.

The tank/baffle/counter electrode assembly was then lowered and the propeller was removed and washed. The solution was covered for the following day's use.

RESULTS AND DISCUSSION

Representative current–voltage data are shown in Fig. 4, for potential sweeps at 0 and 43 rpm. There are two scales for the abscissa. There is arbitrariness in the selection of 1.0 V (negative to Ag–AgCl electrode) as the potential at which limiting current is obtained, but even so, the limiting current is determinable within $\pm 3\%$. The irregularities in the curve at the inflection may actually imply step-wise reduction of oxygen to hydroxyl ion, but there was no attempt to examine such mechanisms.

Data obtained were first plotted as a mass-transfer coefficient, mA/(cm^2 ppm$_{O_2}$), against rpm to test consistency and then transformed to Sherwood Number vs Reynolds Number plots.

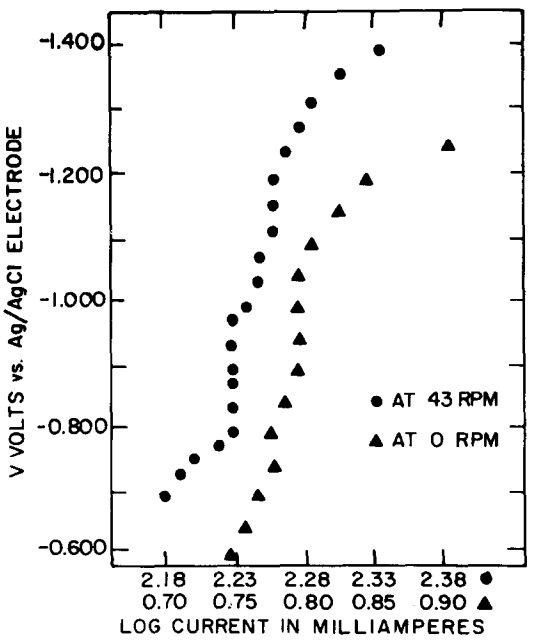

FIG. 4. Typical polarization curves.

Rotating rod

Mass-transfer results are presented in Fig. 5 for experiments that were carried out with a cylindrical rod that rotated with an angular velocity ω about a supporting shaft (cf. Fig. 6). The two ends of the rod were coated with Epoxy so that there was no mass transfer to these surfaces. The tests were carried out at a temperature of 21°C ($Sc = 470$).

Before predictions of the mass transfer are made, the transport over the cylinder is first discussed. Observing the surface of the cylinder after a test was made revealed significant surface discoloration. In particular, the surface had a red–brown color in the darkened areas shown in Fig. 7a. It is noted that prior to a test the surface was that of shiny, polished brass. The dark zone labeled (1) corresponds to the high mass transfer, small boundary-layer thickness region where the fluid first comes into contact with the cylinder. The darkened zone is more extensive at the larger distances from the axis of rotation where the velocities and the mass transfer are larger. As the fluid moves across the cylinder the boundary layer increases, and there is a decrease in the mass transfer corresponding to the light area marked (2). In general, the region near the outermost tips of the rod exhibits increased mass transfer [note region (3)] while the innermost area near the shaft shows little surface change.

Calculations were made of the heat or mass transfer based on cross-flow results for stationary test specimens. The component of velocity in the radial direction was neglected. The results of Krujilin as reported by Morgan [1] and by Perkins and Leppert [1, 2] were used to obtain a local Sherwood (Nusselt) number based on a local Reynolds number, $x\omega D/\nu$, x being measured along the length of the cylinder (refer to Fig. 6). An overall or average Sherwood number was then obtained by integration, viz:

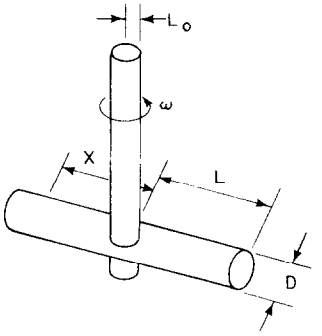

FIG. 6. Schematic drawing of cylindrical rod.

$$Sh = \frac{1}{L-L_0}\int_{L_0}^{L} Sh(x)\mathrm{d}x. \tag{1}$$

The following results were obtained with $Re_L = L\omega D/\nu$, $Re_{L_0} = L_0\omega D/\nu$:

Krujilin:

$$Sh = \frac{0.169}{L-L_0}\left[L\cdot Re_L^{0.6} - L_0\cdot Re_{L_0}^{0.6}\right]\left(\frac{Sc}{0.71}\right)^{1/3},$$

$$6.0\cdot 10^3 < Re_L < 1.3\cdot 10^5. \tag{2}$$

Perkins and Leppert:

$$Sh = \frac{1}{L-L_0}\left[0.175\,(L\cdot Re_L^{0.5} - L_0\cdot Re_{L_0}^{0.5})\right.$$

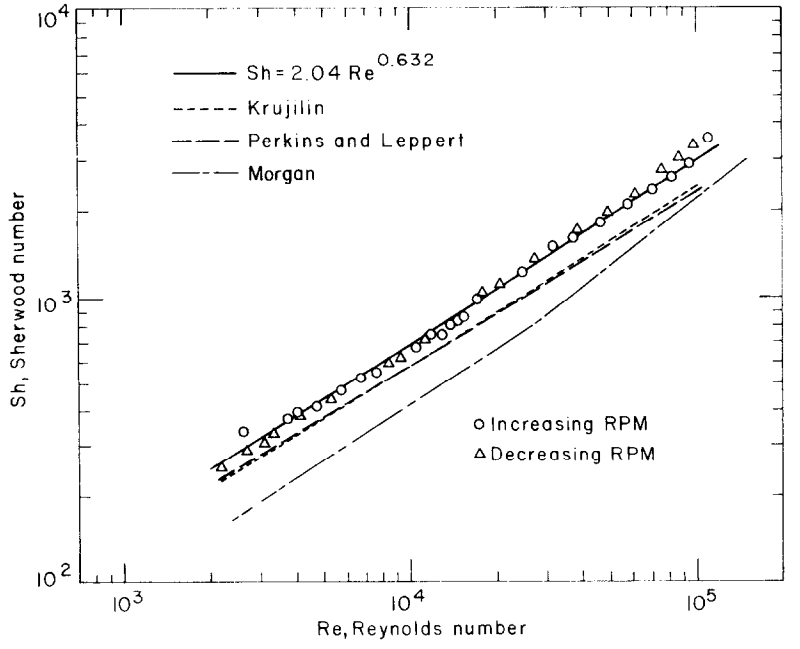

FIG. 5. Mass-transfer results for cylindrical rod.

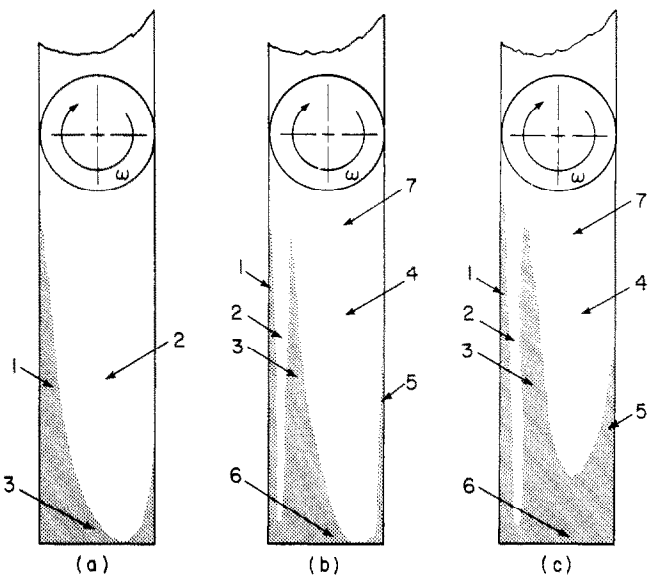

FIG. 7. Sketch of surface discoloration of (a) cylindrical rod, (b) flat plate, and (c) pitched flat plate.

$$+0.0522(L\cdot Re_L^{0.67}-L_0Re_{L_0}^{0.67})]\left(\frac{Sc}{0.71}\right)^{1/3},\qquad 40<Re_L<10^5. \quad (3)$$

Morgan:

$$Sh=\frac{0.0906}{L-L_0}[L\cdot Re_L^{0.633}-L_0\cdot Re_{L_0}^{0.633}]\left(\frac{Sc}{0.71}\right)^{1/3},\qquad 5\cdot10^3<Re_L<5\cdot10^4,$$

$$Sh=\frac{1}{L-L_0}[0.0115(L\cdot Re_L^{0.814}-L^*(50\,000)^{0.814})+0.0906(L^*(50\,000)^{0.633}-L_0Re_{L_0}^{0.633})]\left(\frac{Sc}{0.71}\right)^{1/3}, \quad (4)$$

$$5\cdot10^4<Re_L<2\cdot10^5$$

where L^* is the location where $L^*\omega D/\nu = 50\,000$. These results are shown in Fig. 5. The data may be correlated according to (cf. Fig. 5):

$$Sh=2.04Re^{0.632}=2.04\left[\left(\frac{L+L_0}{2}\right)\frac{\omega D}{\nu}\right]^{0.632}\qquad \text{at}\quad Sc=470. \quad (5)$$

It is seen that all results from the cross-flow stationary cylinder analogy, equations (2), (3) and (4) are less than the experimental data. It is possible that this may be due to the effect of the baffles on the mass transfer but no attempt was made to include this effect in the analysis. Also prominent is the increased mass transfer at Reynolds numbers above 10^5 which corresponded to the increased air entrainment associated with a Rankine vortex formation.

For completeness, equation (5) is extended to other Schmidt numbers by assuming a $Sc^{1/3}$ dependence so that

$$Sh=0.263\left[\left(\frac{L+L_0}{2}\right)\frac{\omega D}{\nu}\right]^{0.632}Sc^{1/3}. \quad (6)$$

Rotating plate

Experiments were also carried out with a plate or blade (dimensions given under Experimental System) that is rotating with an angular velocity ω about a supporting shaft (cf. Fig. 8) and these data are presented in Fig. 9. The two ends of the plate were coated with Epoxy so that there was no mass transfer to these surfaces. The tests were carried out at a temperature of 23°C ($Sc = 440$) and the data were correlated by the relation

$$Sh=0.728Re^{0.711}=0.728\left[\left(\frac{L+L_0}{2}\right)\frac{\omega B}{\nu}\right]^{0.711}\qquad \text{at}\quad Sc=440. \quad (7)$$

The condition of the surface of the plate after a test revealed significant surface discoloration as sketched in Fig. 7b. The fluid first comes into contact with the plate at a rounded leading edge and in this region, zone (1) the boundary layer is thin, the mass-transfer rate is

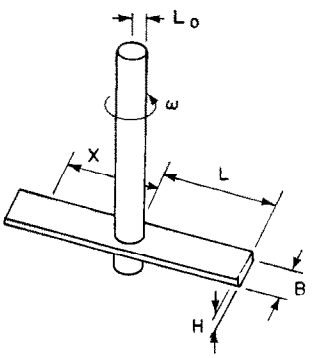

FIG. 8. Schematic drawing of flat plate.

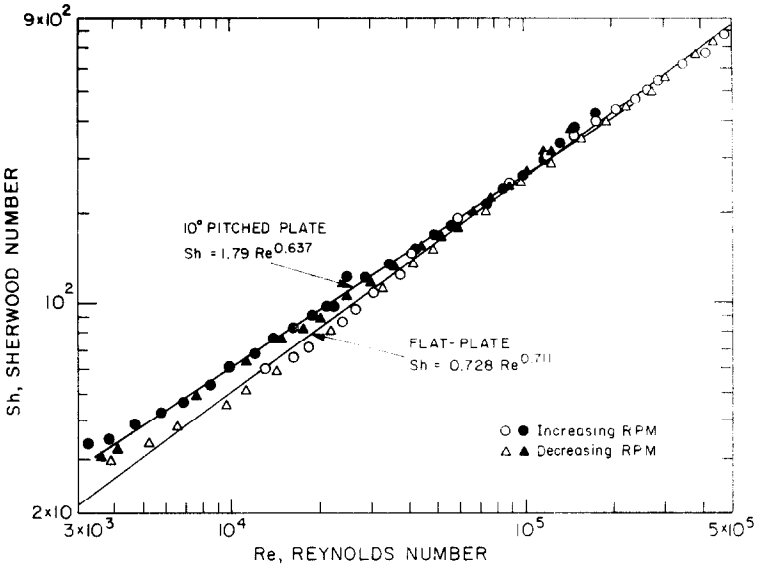

FIG. 9. Mass-transfer results for flat plate and flat plate with 10° pitch. Darkened symbols are for plate with pitch.

high and a red–brown surface is observed. As the fluid proceeds along the plate there is a decrease in the mass transfer corresponding to zone (2) which shows little surface change. Continuing across the plate a red-brown surface is again present, zone (3), which may be due to the initiation of turbulence. After the turbulent flow is developed the mass transfer again decreases and leads to zone (4) which has little surface change. In zone (5), the trailing edge region away from the supporting shaft, there is another area of increased mass transfer as well as at the outermost tips of the plate, zone (6). Note that the innermost region of the plate, zone (7), which has the lowest speeds, shows little surface change.

Equation (7) is extended to other Schmidt numbers according to

$$Sh = 0.096\left[\left(\frac{L+L_0}{2}\right)\frac{\omega B}{\nu}\right]^{0.711} Sc^{1/3}. \qquad (8)$$

It is noted that calculations were made for the mass transfer based on cross-flow results for stationary test specimens in the manner presented for the rotating rod. The results from these calculations were in poor agreement with the data and have not been presented here. The details of this effort are given by Teng [8].

Rotating pitched plate

Experiments were also carried out with a plate (dimensions given under Experimental Systems) pitched at 10° and these data are presented in Fig. 9. The two ends of this plate were also coated with Epoxy so that there was no mass transfer to these surfaces. The data may be correlated according to

$$Sh = 1.79Re^{0.637} = 1.79\left[\left(\frac{L+L_0}{2}\right)\frac{\omega B}{\nu}\right]^{0.637} \quad \text{at} \quad Sc = 440. \qquad (9)$$

for tests that were carried out at a temperature of 23°C ($Sc = 440$). The sketch of the upper surface of the plate after a test (cf. Fig. 7c) shows a trend that is similar to that previously discussed for the plate at zero pitch. The changes for the upper surface are more pronounced for the pitched plate while the lower surface exhibited a fairly uniform light discoloration.

Equation (9) is extended to other Schmidt numbers according to

$$Sh = 0.236\left[\left(\frac{L+L_0}{2}\right)\frac{\omega B}{\nu}\right]^{0.637} Sc^{1/3} \qquad (10)$$

CONCLUSIONS

Three vertically-mounted brass shapes were rotated in aerated 3.5% salt solution at temperatures of 21°C and 23°C and polarization curves were obtained. Results for the mass transfer were then determined and the data correlated according to:

$$Sh_{\text{cylindrical rod}} = 2.04Re^{0.632} \quad \text{at} \quad Sc = 470,$$
$$2 \times 10^3 < Re < 10^5,$$
$$= 0.263Re^{0.632}Sc^{1/3},$$
$$Sh_{\text{flat plate}} = 0.728Re^{0.711} \quad \text{at} \quad Sc = 440,$$
$$4 \times 10^3 < Re < 5 \times 10^5,$$
$$= 0.096Re^{0.711}Sc^{1/3},$$
$$Sh_{\text{flat plat, 10° pitch}} = 1.79Re^{0.637} \quad \text{at} \quad Sc = 440,$$
$$3 \times 10^3 < Re < 2 \times 10^5,$$
$$= 0.236Re^{0.637}Sc^{1/3}.$$

Using these correlations the maximum corrosion rates may be calculated as well as the current required for cathodic protection. Note that for the rod, $Re = (L+L_0)\omega D/2\nu$ and for the plates $Re = (L+L_0)\omega B/2\nu$.

Acknowledgement—The authors acknowledge with appreciation the partial support of this research by the Sea Water Conversion Laboratory and the Lawrence Berkeley Laboratory, University of California. The authors also express appreciation to Peter Loh and John Kan, graduate students who took the data.

REFERENCES

1. V. T. Morgan, The overall convective heat transfer from smooth circular cylinders, *Advances in Heat Transfer*, (edited by T. J. Irvine, Jr. and J. P. Hartnett) Vol. 11, pp. 199–264. Academic Press, New York (1975).
2. H. C. Perkins, Jr. and G. Leppert, Forced convection heat transfer from a uniformly heated cylinder, *J. Heat Transfer* **84**, 257–263 (1962).
3. V. G. Levich, *Physicochemical Hydrodynamics*, Chapter VI (Translated by Scripta Technica) Prentice-Hall, New York (1962).
4. C. W. Tobias, M. Eisenberg and C. R. Wilke, Diffusion and convection in electrolysis—a theoretical review, *J. Electrochem. Soc.* **99**, 395c (1952).
5. P. Delahay, *New Instrument Methods in Electrochemistry*, New York (1954).
6. J. Newman, *Electrochemical Systems*, Prentice-Hall, New York (1973).
7. J. T. Teng, R. Greif, I. Cornet and R. N. Smith, Study of heat and mass transfer in pipe flows with non-Newtonian fluids, *Int. J. Heat Mass Transfer* **22**, 493–498 (1979).
8. J. T. Teng, Experimental and Theoretical Studies in Convective Transport, Ph.D. Dissertation, University of California, Berkeley (1978).

TRANSFERT MASSIQUE AUTOUR DE CYLINDRES ET DE PLAQUES EN ROTATION

Résumé—Des résultats expérimentaux sont présentés pour le transfert massique autour de plaques et de cylindres tournants. On considère les régimes d'écoulement et leur effet sur le transfert de masse. Une procédure de calcul basée sur une analogie de l'écoulement transversal autour d'un cylindre fixe est considérée et elle est comparée avec les résultats expérimentaux.

STOFFÜBERGANG AN ROTIERENDE ZYLINDER UND PLATTEN

Zusammenfassung—Für den Stoffübergang an rotierende Zylinder und Platten werden experimentelle Ergebnisse mitgeteilt. Strömungszustände und deren Einfluß auf den Stoffübergang werden erläutert. Eine auf der Analogie zum ruhenden Zylinder im Kreuzstrom basierende Rechnung wird beschrieben und mit Versuchswerten verglichen.

МАССОПЕРЕНОС К ВРАЩАЮЩИМСЯ СТЕРЖНЯМ И ПЛАСТИНАМ

Аннотация — Представлены результаты экспериментального исследования переноса массы к вращающимся стержням и пластинам. Отмечено влияние различных режимов течения на перенос массы. Приведен расчет, основанный на аналогии с поперечным обтеканием неподвижного цилиндра, и дано сравнение с экспериментальными данными.